Relationship between aerosol and cloud fraction over Australia

Jennifer D. Small,[1] Jonathan H. Jiang,[1] Hui Su,[1] and Chengxing Zhai[1]

Received 30 August 2011; revised 20 October 2011; accepted 26 October 2011; published 2 December 2011.

[1] We study the relationships between aerosols, clouds, and large scale dynamics over a north coastal Australia (NCA) region and a southeast Australia (SEA) region during the period 2002–2009 to evaluate the applicability of the aerosol microphysics-radiation-effect (MRE) theory proposed by Koren et al. (2008) in a low aerosol environment. We use aerosol optical depth (τ_a), fire counts, and cloud fraction (f_c) from Aqua-MODIS, and NCEP Reanalysis vertical velocities at 500 mb (ω_{500}) as a proxy for dynamic regime. In the NCA we find a monotonic increase f_c (35%, absolute f_c) as a function of increasing τ_a. In the SEA, we find that f_c initially increases by 25% with increasing τ_a, followed by a slow systematic decrease (~18%) with higher τ_a. We show that the MRE theory proposed by Koren et al. (2008) adequately represents the variation of f_c with τ_a in both the NCA and SEA. By conditionally sorting data by ω_{500} we investigate the role dynamics plays in controlling the τ_a-f_c relationship and the rate at which f_c changes with τ_a. We find that the MRE theory can be used to empirically fit both $-\omega_{500}$ and $+\omega_{500}$ observations. By analyzing meteorological parameters from the NCEP Reanalysis, we find that variations in local meteorology are not likely the cause of the observed relationships of τ_a and f_c during biomass burning seasons. However, additional factors such as aerosol type and cloud type may play a role. **Citation:** Small, J. D., J. H. Jiang, H. Su, and C. Zhai (2011), Relationship between aerosol and cloud fraction over Australia, *Geophys. Res. Lett.*, *38*, L23802, doi:10.1029/2011GL049404.

1. Introduction

[2] Absorbing aerosols, including biomass burning smoke and dust, affect large regions of the globe with the potential to influence and modify clouds [*Koch and Del Genio*, 2010]. The study of aerosol effects on clouds is complex and their interaction may be influenced or obscured by regional and local meteorology and dynamics [*Ten Hoeve et al.*, 2011]. In both theoretical and observational studies, cloud properties (both micro- and macro-physical) are found to be influenced by atmospheric aerosol loading. For example, cloud fraction (f_c) is thought to vary as a function of aerosol amount, with some researchers reporting an increase in f_c with increasing aerosol optical depth [*Feingold et al.*, 2001; *Loeb and Schuster*, 2008; *Koren et al.*, 2010], while others, using aircraft observations, find that f_c can actually decrease in the presence of increased aerosol [*Small et al.*, 2009] and result in changes in cloud lifetime. Consequently, the aerosol "lifetime effect," in which increased aerosol results in higher cloud drop concentration, increased liquid water paths, cloud fraction, and higher albedo and thus longer cloud lifetime, has come under scrutiny in recent years. Local meteorology and dynamics are theorized to play several roles in modifying aerosol effects on clouds and precipitation via various pathways, including available precipitable water, relative humidity, and updraft velocities [*Loeb and Schuster*, 2008; *Dey et al.*, 2011]. *Yuan et al.* [2008] found that available water vapor explained 70% of the variance in the slope of the correlation found between drop effective radii and aerosol optical depth in their coastal study regions, while *Feingold et al.* [2001] found it had limited effect on their study of biomass burning aerosols in Brazil. *Ten Hoeve et al.* [2011] found that background column water vapor likely exerts a strong effect on cloud properties. High relative humidity (RH) at cloud base has been associated with positive correlations between cloud fractions and aerosol optical depth [*Loeb and Schuster*, 2008]. Changes in the local dynamics can also modify cloud microphysics and how the cloud system responds to aerosols. To prevent contamination by meteorological factors previous studies employ various techniques intended to cancel out or limit their effects such as spatial and temporal averaging or specific sorting and filtering criteria [*Kaufman and Nakajima*, 1993; *Loeb and Schuster*, 2008; *Huang et al.*, 2009; *Grandey and Stier*, 2010]. Recently, *Koren et al.* [2008] put forth a theory that predicts both an increase and decrease in f_c with τ_a. We refer to this theory here as the combined microphysical–radiative effect, or MRE. For the microphysical component, when τ_a increases f_c increases exponentially until the effect saturates at large τ_a. For the radiative component, absorbing aerosols interact with incoming solar radiation within the aerosol layer. This reduces the amount of solar radiation reaching the surface, stabilizing the boundary layer via heating within the cloud layer, suppressing cloud formation and decreasing f_c. By incorporating both the microphysical response of clouds and the radiative changes to the cloud layer in the presence of aerosols the MRE accounts for an initial increase followed by decrease in f_c as aerosol loading is increased. Due to the regional nature of aerosols and fire occurrence, it is necessary to focus on locations within specific dynamic and meteorological regimes. Thus, this work provides an analysis of two study regions in Australia, a north coastal region (NCA) and southeastern coastal region (SEA). Both regions have active fire seasons and are periodically influenced by dust from the central Australian Desert. This analysis combines observations of aerosols and clouds from satellite and reanalysis data sets to address unanswered questions related to aerosol-cloud interactions. Focusing on peak biomass burning seasons increases the potential amount of absorbing aerosols and reduces the influence of seasonal variability. We seek to minimize the influence of large-scale meteorology by restricting the spatial and temporal domains in which the aerosol and cloud properties are compared by choosing small study regions and daily data for select seasons.

[1]Jet Propulsion Laboratory, California Institute of Technology, Pasadena, California, USA.

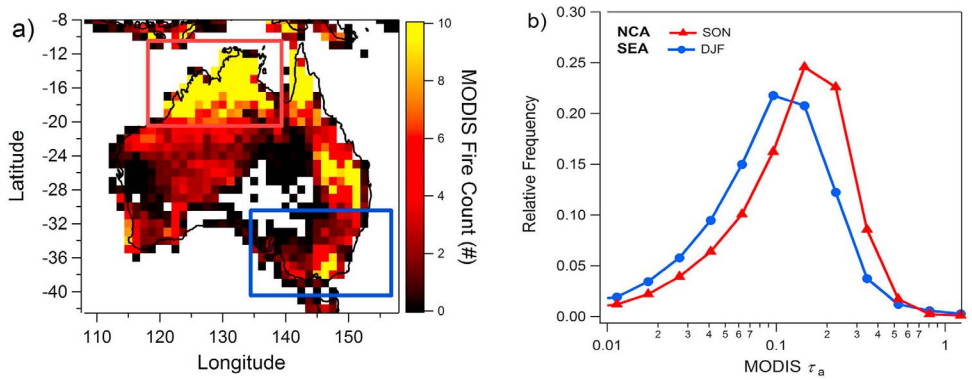

Figure 1. Climatological (a) Aqua MODIS Fire Counts based on monthly data from July 2002-December 2009 with NCA (red box) and SEA (blue box) outlined, (b) relative frequency of MODIS AOD for the NCA (red triangles) and the SEA (blue dots).

The primary questions to be addressed are: How does cloud fraction vary as a function of aerosol? What impact do local dynamics have on this relationship?

2. Data

[3] We use globally gridded daily data sets standardized to a 1 × 1.25° grid by linear interpolation for the ~8 year period July 2002 to December 2009. We use seasonal subsets from the full data record, focusing solely on the dry seasons with definite biomass burning activity to maximize the potential presence of absorbing aerosols and limit meteorological variability. For aerosol, we use daily Level-3 globally gridded aerosol optical depth (τ_a) from the *MOD*erate *R*esolution *I*maging *S*pectroradiometer (MODIS) on the Aqua satellite (MYD08_M3, MYD08_D3, Collection 5.1) [*Remer et al.*, 2008]. In depth discussions of MODIS τ_a are given by *Chu et al.* [2002], *Levy et al.* [2005], and *Lin et al.* [2006]. Following *Torres et al.* [2010], we use monthly MODIS fire count data, to identify locations and occurrence of fire activity. We also use aerosol classification data from the Cloud-Aerosol Lidar and Infrared Pathfinder Satellite Observations satellite (CALIPSO) [*Winker et al.*, 2007] and Aerosol Index (AI) observations from the Ozone Monitoring Instrument (OMI) [*Torres et al.*, 2007] to confirm that absorbing aerosol (pure smoke, dust and polluted dust) are present during the seasons chosen in this study. We use daily Level-3 MODIS f_c, obtained by calculating global cloud amounts from instantaneous cloud masks [*Platnick et al.*, 2003]. Following *Koren et al.* [2008], we use Level-3 MODIS cloud top pressures (CTP) as a measure of cloud vertical development. Since aerosols and clouds are influenced by local and regional meteorology we use daily regridded NCEP Reanalysis data [*Kalnay et al.*, 1996] to set the meteorological and dynamical context. Specifically, we use vertical velocities at 500 mb (ω_{500}) to account for differences in large scale dynamics and evaluate precipitable water (PW) and relative humidity (RH) as a function of aerosol to account for differences in available water vapor.

3. Study Area

[4] MODIS fire count data are used to characterize the timing and location of biomass burning and to choose our regions of interest and maximize the amount of absorbing aerosols present. Figure 1a shows the geographic distribution of mean fire activity from July 2002 to December 2009. An analysis of the annual cycle of biomass burning (not shown) identifies the peak biomass burning seasons as SON for the NCA and DJF for the SEA. To assess the variability in the τ_a-f_c relationship we choose regions with distinctly different meteorological conditions with well defined fire seasons and activity: a) the NCA defined by 10.5°S to 20.5°S and 118.125°W to 139.375°W and b) the SEA defined by 30.5°S to 50.5°S and 134.375°W to 156.875°W. Figure 1b shows the relative frequency of MODIS τ_a for each region. The mean ($\pm\sigma$) for τ_a for NCA during SON (2002–2009) is 0.16 ± 0.16 and for SEA during DJF (2002–2009) is 0.12 ± 0.17.

[5] Our study regions are dominated by absorbing biomass burning aerosols and dust from the central desert. CALIPSO aerosol data sorted by aerosol type is used to determine the percentage of aerosol considered to be absorbing (75% in the NCA and 65% in the SEA). Comparisons between MODIS τ_a and OMI AI for the selected seasons further confirms the presence of absorbing aerosols, see auxiliary material for additional information.[1] In comparison to other biomass burning regions such as Africa and South America, the Australian continent has a very low total aerosol amount [*Remer et al.*, 2008].

[6] Cloud characteristics, such as f_c, are also affected by the large scale (synoptic) patterns [e.g., *Dey et al.*, 2011] of the region in which they are formed. Australia is characterized by monsoonal activity in the north and by mid-latitude storms in the south. However, by choosing biomass burning seasons, meteorological variability is reduced as can bee seen in Figures 2a–2c. Here we see that three indicators of local meteorology, ω_{500}, PW and RH, show very little dependence on τ_a. This suggests that meteorological conditions are stable for the chosen seasons and we conclude that variations in local meteorology should not play a large role in determining the relationship between τ_a and f_c. During the SON study period NCA has

[1] Auxiliary materials are available in the HTML. doi:10.1029/2011GL049404.

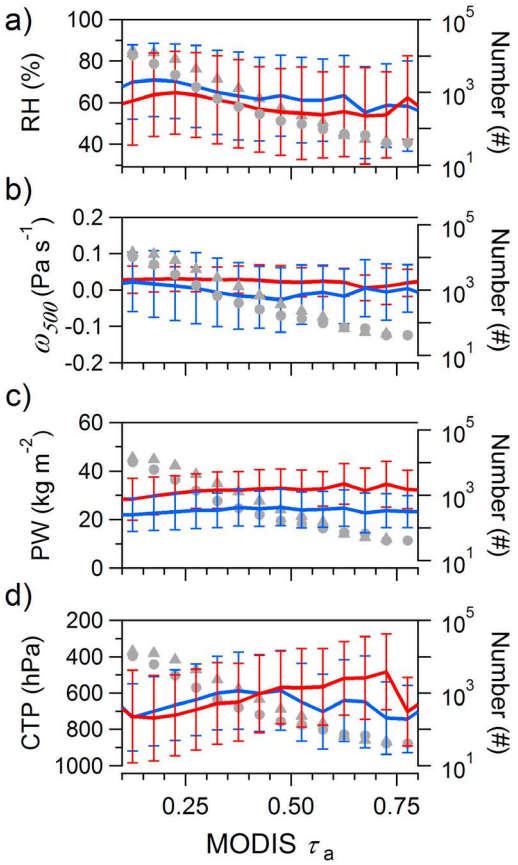

Figure 2. Meteorological parameters, (a) ω_{500} (Pa s^{-1}), (b) PW (kg m^{-s}), (c) RH (%), and (d) MODIS cloud top pressure (hPa) $\pm 1\sigma$ sorted as a function of MODIS τ_a for the two regions: NCA (red curves) and SEA (blue curves). Number of samples in each bin are represented by grey triangles (NCA) and dots (SEA).

a mean ($\pm\sigma$) f_c of 0.29 ± 0.15, while during DJF the SEA has a mean ($\pm\sigma$) f_c of 0.57 ± 0.14.

4. Results

4.1. Observed Relationships Between f_c and τ_a

[7] In this section we examine the relationships between τ_a and f_c during the fire seasons SON and DJF for the NCA and SEA regions, respectively, for the eight year period 2002–2009. Figures 3a and 3b show f_c sorted into linearly spaced τ_a bins for the NCA and SEA respectively. We only show data for $0 < \tau_a < 0.8$ due to the limited number of samples for $\tau_a > 0.8$ and to avoid potential misclassification of clouds and aerosols (following *Koren et al.* [2008]).

[8] For the NCA, f_c increases consistently with τ_a for $0 < \tau_a < 0.6$ at rate of 6% per 0.1 increase in τ_a. When $\tau_a > 0.6$, f_c decreases slightly with increasing τ_a, per bin for $\tau_a > 0.6$. However, there are not enough samples to provide a statistically significant sample for $\tau_a > 0.6$. The peak f_c is 60% when τ_a is 0.6. For the SEA we see that when τ_a is relatively small ($0 < \tau_a < 0.3$), f_c increases with τ_a more dramatically than in the NCA with a rate of 10% per 0.1 increase in τ_a. When $0.3 < \tau_a < 0.8$, f_c decreases at a rate of 3.5% per 0.1 increase in τ_a. The peak f_c in the SEA is ~70% when τ_a is 0.3. The differences in f_c response to τ_a in the NCA and the SEA regions will be addressed in Section 5.

[9] The relationship between τ_a-f_c for the SEA approximately resembles the theoretical prediction of the MRE and the competing effects of the aerosol microphysical and radiative effects. The radiative component of the MRE, results in a steady, linear decrease in f_c as a function of increasing aerosol. An analysis of the data suggests that the initial f_c is key in determining the slope of the decrease in f_c [see *Koren et al.*, 2008, Figure 1] with increasing aerosol. The strength of the radiative component of the MRE can be described as the absolute change in f_c and is the difference between the peak f_c and the value of f_c at a maximum τ_a (in this case $\tau_a = 0.8$), represented here by Δf_c. Referring to Figure 3b an analysis of the τ_a-f_c relationship for SEA shows evidence of a radiative effect in f_c with a Δf_c decrease of ~18% over the $0.3 < \tau_a < 0.8$ range. The MRE also predicts that the lower (higher) the initial cloud fraction, the stronger (weaker) the radiative effect resulting in a larger (smaller) decreasing slope. However, for the NCA the observations in Figure 3a more closely resemble those in Figure 2 of *Koren et al.* [2005], in which they found a consistent monotonic increase in f_c as τ_a increased from 0 to 0.5 over a North Atlantic region. Since there is no clear evidence of a radiative effect in the NCA, we focus primarily on the microphysical effect for the NCA.

4.2. Observed Relationships With τ_a as a Function of ω_{500}

[10] Dynamics play a large role in determining cloud properties and one of the fundamental differences between the NCA and the SEA is the difference in the general dynamics of the two regions. Based on climatological lower tropospheric stability calculated using NCEP Reanalysis temperature data at 1000 and 700 mb, (not shown), on an annual basis the NCA (SEA) is characterized as less stability (more stability) and lower (higher) cloud fraction. Here we investigate how dynamics, using $-\omega_{500}$ as a proxy, affects the observed relationships between τ_a and f_c (refer back to Figure 2b).

[11] In Figure 3b we clearly see the effect of dynamics on the observed relationships between τ_a and f_c for each region. For the NCA we see that the rate of increase in f_c with increasing τ_a, is similar for both $+\omega_{500}$ (descending) and $-\omega_{500}$ (ascending). However, $-\omega_{500}$ samples have characteristically higher f_c. In the SEA there is a slight difference between the initial rates of increase in f_c for data classified by + and $-\omega_{500}$. For + and $-\omega_{500}$, over the range of $0 > \tau_a > 0.3$, f_c increases by ~12% for $+\omega_{500}$ and only ~8% for $-\omega_{500}$. In the SEA, $-\omega_{500}$ shows fairly constant f_c for $\tau_a > 0.3$ and those with $+\omega_{500}$ show a 25% decrease in f_c for $0.3 < \tau_a < 0.8$.

[12] Possible causes for the differences between + and $-\omega_{500}$ regimes include: (1) for subsidence regimes, in the SEA, ($+\omega_{500}$), aerosols may remain close to the surface, and as suggested by *Koren et al.* [2008], heat the sub-cloud and cloud layer and stabilize the boundary layer. Boundary layer stabilization suppresses cloud formation thus reducing f_c; (2) In the NCA, convection ($-\omega_{500}$), can increase cloud amount, increasing the initial f_c. In the SEA, additional convection may lower clear-sky percentages and decrease the potential impact of the aerosol radiative effect, preventing f_c from decreasing as efficiently with increasing τ_a.

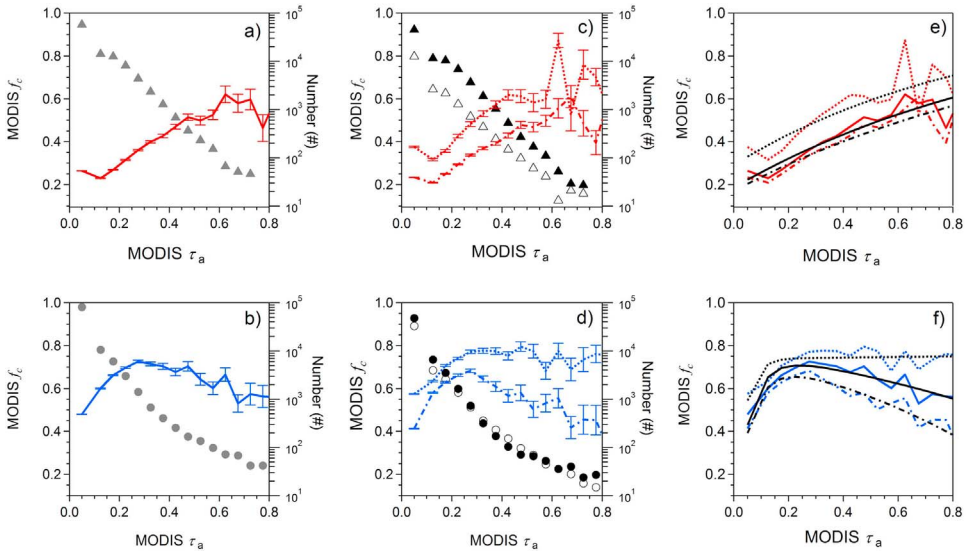

Figure 3. MODIS f_c as a function of τ_a for (a) NCA (red) and (b) SEA (blue), and conditionally sorted by + and $-\omega_{500}$ (c) for NCA and (d) for SEA. Vertical bars show standard errors for each aerosol bin. Dashed red and blue lines are for $-\omega_{500}$ and dashed-dotted red and blue lines are for $+\omega_{500}$ are for NCA and SEA regions respectively. Grey triangles (NCA) and dots (SEA) show number of samples in each τ_a bin. (e) Same as in Figures 3a and 3c with empirically fit curves (black) overlain. (f) Same as in Figures 3b and 3d with empirically fit curves (black) overlain. For both Figures 3d and 3e empirical fit curves depict the f_c dependence on the superposition of the microphysical and radiative effects (line styles same as described above for all, $+\omega_{500}$, and $-\omega_{500}$ data).

[13] Referring again to Figures 3c and 3d and considering the absolute change in f_c, we see that for the NCA, ω_{500} sorted f_c show similar microphysical effects with increases of ~30% for both + and $-\omega_{500}$. For ω_{500} sorted f_c in the SEA, we see a weak absorption effect for the $-\omega_{500}$ sorted data (highest maximum f_c) with a Δf_c of ~0% and $+\omega_{500}$ (lowest maximum f_c) data showing the strongest radiative effect with a Δf_c of ~20%. These findings are consistent with the MRE and predictions described above.

[14] In addition to the absolute change in f_c, which aids in identifying differences within the same region, *Koren et al.* [2008] also define the relative change in f_c as $\Delta f_c/\max(f_c)$. The relative change in f_c, which is normalized by the maximum f_c, allows for the comparison between regions. For our data we find the relative increase in f_c is greater for the NCA (0.58) than the SEA (0.35) with a relative decrease in the SEA of 0.25. In the SEA, as theoretically predicted, we observe a stronger aerosol radiative effect in response to aerosol (at high τ_a) for $+\omega_{500}$ as compared to $-\omega_{500}$. Thus, it is observed that regimes with lower initial f_c are more susceptible to the radiative effect than regimes with higher initial f_c.

4.3. Empirical Fitting

[15] Based on the theoretical predictions of the MRE, *Koren et al.* [2008] find a continuous transition in the relationship between f_c and τ_a from a microphysically affected regime at low τ_a and a radiative affected regime at high τ_a. Here we evaluate the MRE in the two selected regions affected by absorbing aerosols (including both dust and smoke) with average τ_a values lower than that observed over the Amazon as in *Koren et al.*'s [2008] study.

[16] We begin by fitting our f_c curves for NCA and SEA with equation (5) of *Koren et al.* [2008] to test the logarithmic response of the f_c to microphysical effects (not shown separately). We re-write equation (5) of *Koren et al.* [2008], to be consistent with our nomenclature, as:

$$f_{cm} = f_{cs}\left(1 - \exp\left(-\frac{1}{b_f}\tau_a\right)\right) \quad (1)$$

where f_{cm} is the cloud fraction under the influence of the microphysical effect, f_{cs} is the maximum cloud fraction at which the microphysical effect saturates, τ_a is the aerosol optical depth and b_f is a parameter determining the slope of the increase in f_c. Values for the fitting parameters b_f and f_{cs} can be found in Table 1, derived from least-square fits for the combined microphysical and radiative effect.

[17] As mentioned above, in addition to the microphysical effect, *Koren et al.* [2008] explain the reduction in f_c at higher τ_a as the result of an aerosol radiative effect. The radiative effect is an exponential dependence of f_c on temperature (influenced by τ_a) resulting in decreasing f_c with increasing τ_a. For the radiative effect we re-write equation (4) of *Koren et al.* [2008]:

$$f_{ca} = 1 - (1 - f_{c0})\exp(-\gamma\tau_a) \quad (2)$$

where f_{ca} is the f_c resulting from the aerosol radiative effects. It is dependent on the amount of clear sky present ($1\text{-}f_{c0}$),

Table 1. Fitted Parameters for f_c Using the Superposition of Equations (5) and (6) of *Koren et al.* [2008]

Region	Fitted Parameter		
	b_f	f_{cs}	γ
NCA	0.0030	0.1867	−0.9056
$+\omega_{500}$	0.0025	0.1707	−0.8135
$-\omega_{500}$	0.0031	0.2292	−1.1112
SEA	0.0566	0.7725	0.8441
$+\omega_{500}$	0.0596	0.7494	1.1262
$-\omega_{500}$	0.0506	0.7523	−0.0514

where f_{c0} is the initial cloud fraction and γ, a proportionality constant, in place of a, Q and t, in the original work by *Koren et al.* [2008]. A combined variable is suitable for this study since we are not specifically investigating the sensitivity of f_c to temperature changes (a), the dependence of aerosol optical properties (Q), or the characteristic time response to aerosols (t). Values for the fitting parameter γ can be found in Table 1.

[18] To determine the total aerosol MRE on f_c we use of equation (6) from *Koren et al.* [2008]:

$$f_{c*} = 1 - \left(1 - f_{cs}\left(1 - \exp\left(-\frac{1}{b_f}\tau_a\right)\right)\right) * \exp(-\gamma\tau_a) \quad (3)$$

The predicted cloud fraction, f_{c*}, is that resulting from the superposition of the microphysical and radiative effects. Taking the analysis further than *Koren et al.* [2008], and following *Jiang et al.* [2010], we perform two dimensional least-squares fitting to the observed data with the empirical formula equation (3), i.e., to determine the parameters f_{cs}, b_f, and γ, through minimizing the following cost function:

$$\underset{f_{cs},b_f,\gamma}{COST} = \sum_i \left[f_c^i - f_c\left(\tau_a^i, f_{cs}, b_f, \gamma\right)\right]^2 \quad (4)$$

where f_c^i is the mean f_c corresponding to the i-th τ_a bin. The τ_a^i is the mean τ_a in the i-th τ_a bin. For our least-squares fitting computation, there are 15 linearly spaced bins of τ_a between 0.05 and 0.775. The least-squares fits are computed using the mean values of f_c derived from the eight fire seasons of MODIS data.

[19] Substituting the fitted parameters into equation (3), we obtain f_c as a function of τ_a for the NCA and SEA (see Figures 3e and 3f). For the NCA we see that the microphysical effect, the rate of increase in f_c, is similar for all samples. This is also by confirmed by close values of b_f, while for the SEA we see slight variations in the rate of increase in f_c, with values of b_f having a broader range (Table 1). The SEA, unlike the NCA, clearly shows evidence of the radiative effect suggesting that the south is more susceptible to the radiative effects of absorbing aerosol. We see that the strongest radiative effect is associated with SEA $+\omega_{500}$, with the lowest value of calculated saturated cloud fraction, f_{cs}. This confirms that low f_c allows for more efficient heating and stabilization of the cloud layer, resulting in further decreases in f_c. We see the weakest absorption effect for SEA $-\omega_{500}$ when f_c is high, preventing surface and cloud layer heating, thus preventing decreases in f_c as τ_a increases. The threshold values for the SEA (when f_c switches from increasing to decreasing) are similar regardless of dynamic regime.

5. Discussion of Regional Differences

[20] We find that the *Koren et al.* [2008] empirical model provides an adequate approximation for the relationship between f_c and τ_a for a range of dynamic conditions. Using this empirical model, we can quantitatively compare the regional differences in the dependence of f_c and τ_a. We find that both the NCA and the SEA exhibit an initial increase in f_c with increased τ_a and that the southern region shows a clear decrease in f_c at highest τ_a. For the SEA, the threshold value of $\tau_a = 0.3$ is within the range of threshold values of 0.2-0.35 found in previous studies [*Koren et al.*, 2008; *Dey et al.*, 2011]. Further studies in additional regions are necessary to better understand what physical processes determine the threshold value. Alternative explanations for the observed correlations between τ_a and f_c are discussed below.

[21] The strong increase in f_c with τ_a found in the NCA is similar to the results of *Koren et al.* [2005] for Atlantic convective clouds primarily affected by dust aerosols, though other effects such as differences in aerosol composition and surface effects on cloud types may also play a role [*Yuan et al.*, 2011]. The NCA is characterized by higher total τ_a, lower mean and maximum f_c, higher PW, and a larger percentage of aerosol categorized as polluted dust (see auxiliary material). Thus, the NCA is affected by a different combination of aerosol types and meteorology than the SEA. One possible scenario to account for the τ_a-f_c relationship in the NCA is that the aerosol contains more particles able to act as CCN and form new clouds (directly increasing f_c) or form additional smaller droplets in existing clouds. These smaller drops may inhibit collision-coalescence and allow the cloud to live longer (maintaining f_c) and potentially deepen as a result of stronger updrafts resulting from latent heat release during condensation [*Koren et al.*, 2005]. We conclude that the microphysical effect (increasing CCN) is the dominant aerosol effect in the NCA since no clear radiative effect is observed. Additional support for the dominance of the CCN effect can be seen in Figure 2d which shows MODIS cloud top pressure (CTP) as a function of τ_a. Here we see a clear indication of decreasing CTP (reversed vertical axis) with increasing aerosol. Like *Koren et al.* [2005], we suggest that this decrease in CTP may be the result of aerosol induced enhancement. Additional work using CTP and cloud top temperature as well as sorting data by cloud type will help clarify the relationship between τ_a and CTP in Australia, but is out of the scope of this study. The empirical fits using equation (3) show the similarities between the dynamic regimes with similar values for b_f and f_{cs}, values dependent on mean f_c such that convective samples have the highest f_{cs}. The negative values for γ are indicative of the fact that the radiative effect is not observed in the NCA.

[22] The characteristic "boomerang" shape observed in the SEA is indicative of the presence of biomass burning aerosols (smoke), as seen in *Koren et al.* [2008], *Ten Hoeve et al.* [2011] and *Dey et al.* [2011]. Indeed, for the SEA, a slightly larger percentage of the absorbing aerosol is classified as smoke (auxiliary material). We also find that f_c behaves predictably in accord with the MRE such that the strongest (weakest) absorption effect is evident for data with the lowest (highest) mean f_c. For the SEA the initial f_c is likely the factor that determines the overall impact of the MRE. When initial f_c is low (high), the radiative (microphysical) effect dominates. The empirical fits suggest that the microphysical effect varies as a function of dynamic regime with $-\omega_{500}$ samples experiencing the strongest microphysical effect. However, since the threshold value (τ_a ~0.3) is similar for all dynamic regimes so are the values of f_{cs} for $+\omega_{500}$ and $-\omega_{500}$ samples. Additionally, γ, our proportionality constant related to optical and thermal properties of the aerosols, changes dramatically as a function of ω_{500}, with a positive value for $+\omega_{500}$ (indicating heating) and a slightly negative value for $-\omega_{500}$ in which little evidence for the radiative effect is found (as in the NCA). For the

SEA, alternative explanations for observed increase in f_c with τ_a may be the result of observed increases in individual cloud number [*Dey et al.*, 2011]. Convective invigoration and cloud deepening may also be acting as well, as we see a slight decrease in CTP (Figure 2d) in the SEA when the microphysical effect is active and then increases in CTP when the radiative effect takes over.

[23] While it is appealing to attribute regional differences observed in the τ_a-f_c relationship solely to an aerosol effect it is necessary to highlight potential alternatives. As stated in the introduction, instrument artifacts, meteorology and local dynamics are thought to play a role in determining both aerosol and cloud characteristics. Numerous recent studies [*Kaufman et al.*, 2005; *Loeb and Schuster*, 2008; *Ten Hoeve et al.*, 2011; *Yuan et al.*, 2011] have attempted to isolate aerosol-cloud interactions finding that in the majority of cases meteorology, dynamics and other factors (such as 3D cloud effects, cloud contamination, and aerosol composition) can be rejected as the dominant player in determining the correlations found between aerosol optical depth and cloud properties. The results presented here suggest that large-scale meteorology is likely not a factor (Figure 2) but we caution that local differences in aerosol type may play a significant role in determining the τ_a-f_c relationship [*Kaufman et al.*, 2005]. Further analysis is necessary to determine how large an impact aerosol type has on the relationship for the chosen study regions. Another critical parameter missing in this analysis is a separation of cloud type. Microphysical processes differ between cloud types and further analysis is necessary to determine if the observed regionally averaged τ_a-f_c relationships are maintained if specific cloud types (cumulus, stratocumulus, cirrus, etc.) are considered separately [*Yuan et al.*, 2011]. Future work will aim to isolate the influences of aerosol type and cloud type.

6. Summary

[24] In this study, a combination of satellite datasets are used to examine the relationships between f_c and τ_a in two meteorologically distinct regions in Australia. We find that in the SEA MODIS f_c generally increases with aerosol loading, followed by a decrease after reaching a threshold value independent of dynamical regime (ω_{500}) and that the NCA shows monotonic increases in f_c with increasing τ_a. Using the empirical formulas put forth by *Koren et al.* [2008] we obtain fit parameters for f_c as a function of τ_a which approximately capture the observed relationships among f_c and τ_a.

[25] The results presented here suggest the importance of regional differences in both f_c amount, aerosol type and in understanding the rates of increase and decrease in cloud cover. Even within the same region dynamics play a role in determining the rates of change in f_c with the more convective regions ($-\omega_{500}$) with higher initial f_c showing the least decrease overall. Choice of region (dynamic and meteorologic setting and likely aerosol type) is important in determining the relationships between aerosols and cloud amount. Thus, generalizations of the relationships between changes in aerosol loading and the effect on cloud properties cannot be made without taking regional differences into consideration. This study provides evidence that the distinct relationship between f_c and τ_a may be explained by the simple MRE model for regions with varying amounts and different types of aerosols. However, it must be noted that cloud particle size, and ultimately cloud fraction, may be influenced by additional factors including fluctuations in aerosol size distributions, and meteorological and dynamical parameters.

[26] **Acknowledgments.** This work was performed at the Jet Propulsion Laboratory, California Institute of Technology, under contract with NASA. We thank the support by NASA Atmospheric Composition Modeling Analysis Program (ACMAP) and the Aura project.

[27] The Editor thanks two anonymous reviewers for their assistance in evaluating this paper.

References

Chu, D. A., Y. J. Kaufman, C. Ichoku, L. A. Remer, D. Tanre, and B. N. Holben (2002), Validation of MODIS aerosol optical depth retrieval over land, *Geophys. Res. Lett.*, *29*(12), 8007, doi:10.1029/2001GL013205.

Dey, S., L. Di Girolamo, G. Zhao, A. Jones, and G. McFarquhar (2011), Satellite-observed relationships between aerosol and trade-wind cumulus cloud properties over the Indian Ocean, *Geophys. Res. Lett.*, *38*, L01804, doi:10.1029/2010GL045588.

Feingold, G., L. A. Remer, J. Ramaprasad, and Y. J. Kaufman (2001), Analysis of smoke impact on clouds in Brazilian biomass burning regions: An extension of Twomey's approach, *J. Geophys. Res.*, *106*, 22,907–22,922, doi:10.1029/2001JD000732.

Grandey, B. S., and P. Stier (2010), A critical look at spatial scale choices in satellite-based aerosol indirect effect studies, *Atmos. Chem. Phys.*, *10*, 11,459–11,470, doi:10.5194/acp-10-11459-2010.

Huang, J., C. Zhang, and J. M. Prospero (2009), Large-scale effect of aerosols on precipitation in the West African Monsoon region, *Q. J. R. Meteorol. Soc.*, *135*, 581–594, doi:10.1002/qj.391.

Jiang, J. H., H. Su, C. Zhai, S. T. Massie, M. R. Schoeberl, P. R. Colarco, S. Platnick, Y. Gu, and K.-N. Lious (2010), Influence of convection and aerosol pollution on ice cloud particle effective radius, *Atmos. Chem. Phys. Discuss.*, *10*, 23,091–23,108, doi:10.5194/acpd-10-23091-2010.

Kalnay, E., et al. (1996), The NCEP/NCAR 40-year reanalysis project, *Bull. Am. Meteorol. Soc.*, *77*, 437–471, doi:10.1175/1520-0477(1996)077<0437:TNYRP>2.0.CO;2.

Kaufman, Y. J., and T. Nakajima (1993), Effect of Amazon smoke on cloud microphysics and albedo—Analysis from satellite imagery, *J. Appl. Meteorol.*, *32*, 729–744, doi:10.1175/1520-0450(1993)032<0729:EOASOC>2.0.CO;2.

Kaufman, Y., I. Koren, L. Remer, D. Rosenfeld, and Y. Rudich (2005), The effect of smoke, dust, and pollution aerosol on shallow cloud development over the Atlantic Ocean, *Proc. Natl. Acad. Sci. U. S. A.*, *102*(32), 11,207–11,212, doi:10.1073/pnas.0505191102.

Koch, D., and A. D. Del Genio (2010), Black carbon semi-direct effects on cloud cover: Review and synthesis, *Atmos. Chem. Phys.*, *10*, 7685–7696, doi:10.5194/acp-10-7685-2010.

Koren, I., Y. J. Kaufman, D. Rosenfeld, L. A. Remer, and Y. Rudich (2005), Aerosol invigoration and restructuring of Atlantic convective clouds, *Geophys. Res. Lett.*, *32*, L14828, doi:10.1029/2005GL023187.

Koren, I., J. V. Martins, L. A. Remer, and H. Afargan (2008), Smoke invigoration versus inhibition of clouds over the Amazon, *Science*, *321*, 946–949, doi:10.1126/science.1159185.

Koren, I., G. Feingold, and L. A. Remer (2010), The invigoration of deep convective clouds over the Atlantic: Aerosol effect, meteorology or retrieval artifact?, *Atmos. Chem. Phys.*, *10*, 8855–8872, doi:10.5194/acp-10-8855-2010.

Levy, R. C., L. A. Remer, J. V. Martins, and Y. J. Kaufman (2005), Evaluation of the MODIS aerosol retrievals over oceans and land during CLAMS, *J. Atmos. Sci.*, *62*, 974–992, doi:10.1175/JAS3391.1.

Lin, J. C., T. Matsui, R. A. Pielke Sr., and C. Kummerow (2006), Effects of biomass-burning-derived aerosols on precipitation and clouds in the Amazon Basin: A satellite-based empirical study, *J. Geophys. Res.*, *111*, D19204, doi:10.1029/2005JD006884.

Loeb, N. G., and G. L. Schuster (2008), An observational study of the relationship between cloud, aerosol and meteorology in broken low-level cloud conditions, *J. Geophys. Res.*, *113*, D14214, doi:10.1029/2007JD009763.

Platnick, S., M. D. King, S. A. Ackerman, W. P. Menzel, B. A. Baum, J. C. Riedi, and R. A. Frey (2003), The MODIS cloud products: Algorithms and examples from Terra, *IEEE Trans. Geosci. Remote Sens.*, *41*(2), 459–473, doi:10.1109/TGRS.2002.808301.

Remer, L. A., et al. (2008), Global aerosol climatology from the MODIS satellite sensors, *J. Geophys. Res.*, *113*, D14S07, doi:10.1029/2007JD009661.

Small, J. D., P. Y. Chuang, G. Feingold, and H. Jiang (2009), Can aerosol decrease cloud lifetime?, *Geophys. Res. Lett.*, *36*, L16806, doi:10.1029/2009GL038888.

Ten Hoeve, J. E., L. A. Remer, and M. Z. Jacobson (2011), Microphysical and radiative effects of aerosols on warm clouds during the Amazon biomass burning season as observed by MODIS: Impacts of water vapor and land cover, *Atmos. Chem. Phys.*, *11*, 3021–3036, doi:10.5194/acp-11-3021-2011.

Torres, O., A. Tanskanen, B. Veihelmann, C. Ahn, R. Braak, P. K. Bhartia, P. Veefkind, and P. Levelt (2007), Aerosols and surface UV products from Ozone Monitoring Instrument observations: An overview, *J. Geophys. Res.*, *112*, D24S47, doi:10.1029/2007JD008809.

Torres, O., Z. Chen, H. Jethva, C. Ahn, S. R. Freitas, and P. Bhartia (2010), OMI and MODIS observations of the anomalous 2008–2009 Southern Hemisphere biomass burning seasons, *Atmos. Chem. Phys.*, *10*, 3505–3513, doi:10.5194/acp-10-3505-2010.

Winker, D. M., W. H. Hunt, and M. J. McGill (2007), Initial performance assessment of CALIOP, *Geophys. Res. Lett.*, *34*, L19803, doi:10.1029/2007GL030135.

Yuan, T., Z. Li, R. Zhang, and J. Fan (2008), Increase of cloud droplet size with aerosol optical depth: An observation and modeling study, *J. Geophys. Res.*, *113*, D04201, doi:10.1029/2007JD008632.

Yuan, T., L. A. Remer, K. E. Pickering, and H. Yu (2011), Observational evidence of aerosol enhancement of lightning activity and convective invigoration, *Geophys. Res. Lett.*, *38*, L04701, doi:10.1029/2010GL046052.

J. H. Jiang, J. D. Small, H. Su, and C. Zhai, Jet Propulsion Laboratory, California Institute of Technology, 4800 Oak Grove Dr., Pasadena, CA 91109, USA. (jennifer.d.small@jpl.nasa.gov)